Spin Quantum Bit with Ferromagnetic Contacts for Circuit QED

Audrey Cottet and Takis Kontos

*Laboratoire Pierre Aigrain, Ecole Normale Supérieure, CNRS (UMR 8551), Université P. et M. Curie,
Université D. Diderot, 24 rue Lhomond, 75231 Paris Cedex 05, France*

We theoretically propose a scheme for a spin quantum bit based on a double quantum dot contacted to
ferromagnetic elements. Interface exchange effects enable an all electric manipulation of the spin and a
switchable strong coupling to a superconducting coplanar waveguide cavity. Our setup does not rely on
any specific band structure and can in principle be realized with many different types of nanoconductors.
This allows us to envision on-chip single spin manipulation and readout using cavity QED techniques.

Achieving a strong coupling between a single atom and
a single photon trapped in a cavity has been instrumental
for studying the interaction of light and matter at the most
elementary level [1]. Recently, what was originally belong-
ing to the realm of quantum optics [2–4] has been brought
into superconducting chips: two level superconducting
circuits (artificial atoms) have been embedded into super-
conducting coplanar waveguide cavities, in the context of
circuit quantum electrodynamics [5]. Extending further
this "transfer" to the field of nanofabricated circuits could
offer a very interesting platform for the study of entangle-
ment and decoherence in many body systems.

The electronic spin of nanoconductors raises a strong
interest in the fields of quantum information and quantum
coherence, because it is generally expected to be more
robust to decoherence than the orbital degrees of freedom
[6]. Coupling the spin of a nanoconductor to cavity photons
seems particularly attractive [7]. Nanofabricated circuits
are naturally compatible with on-chip superconducting
waveguide architectures. However, two major difficulties
have to be overcome. First, a strong coupling g between a
spin and an electric field is intrinsically difficult to achieve.
Second, in architectures integrating several spins, the
selective manipulation of each spin is a challenge. The
electrical schemes available for local spin manipulation
[8–10] and spin-photon coupling [11,12] rely on the use
of a strong external static magnetic field, which is not
naturally compatible with strong photon confinement in
superconducting cavities [13]. More generally, a scheme
allowing one to switch off g efficiently is lacking, for
nanoconductor based qubits as well as superconducting
qubits [14]. An alternative way to spin polarize the spec-
trum of a nanoconductor is to use ferromagnetic insulator
(FI) contacts, which have a very strong internal Zeeman
field. The hybridization of the nanoconductor orbitals with
the first atomic layers of the FIs leads to an effective
Zeeman field inside the nanoconductor itself. This effect
is quite universal since it can arise in very different systems,
such as carbon nanotubes [15–17], InAs quantum dots [18]
or thin superconducting layers [19,20]. In this Letter, we

propose theoretically a scheme for a spin qubit based on a
double quantum dot contacted to ferromagnetic insulators.
Interface exchange effects enable an all electric manipula-
tion of the spin and a switchable strong coupling to a
superconducting cavity. First, our scheme is compatible
with superconducting architectures since it can be realized
using FI layer designs which minimize stray fields. Second,
it is generic in the sense that it does not rely on intrinsic
nanoconductor properties such as spin-orbit coupling [11]
or hyperfine interaction [12]. Third, it is relatively robust
since the contact-induced effective fields can be adjusted in
numerous ways, from the fabrication to the operation of the
quantum dots. This allows us to envision single spin ma-
nipulation and readout using cavity QED techniques.

We first consider two generic quantum dots L and R
coupled through a tunnel barrier with a hopping constant t
(see Fig. 1). Each dot is connected to a grounded normal
metal reservoir through a FI layer, and capacitively coupled
to a dc gate with voltage $V_g^{L(R)}$, which allows us to tune the
chemical potential of the dot. The double dot system is
placed between the center and ground conductors of a
superconducting coplanar waveguide cavity, which con-
veys a voltage V_{ac}. We take into account one orbital level
for each quantum dot. The dots have strong self and
mutual charging energies, so that, by tuning properly V_g^L
and V_g^R, we reach a regime where the total number of
electrons on the double dot system is constantly equal to 1
(see Fig. 2). The tunnel rates through the FIs are sufficiently
small so that cotunneling processes between the dot and the
normal reservoirs can be neglected. Our key ingredient is
the contact-induced effective spin splittings $2\delta_{L(R)}$ in dots
$L(R)$. The effective fields in dots L and R are colinear to the
magnetizations $\vec{m}_L$ and $\vec{m}_R$ of the left and right FIs, which
form an angle θ. For later use, we note $|e_L, e_R\rangle$ a double dot
state with the dot $L(R)$ in state $e_{L(R)}$. Here, $e_{L(R)}$ can be the
empty state $\varnothing$ or a singly occupied state with a given spin
(for instance $\uparrow_{L(R)}$ and $\downarrow_{L(R)}$ refer to spin states parallel
and antiparallel to $\vec{m}_{L(R)}$, respectively). With the above
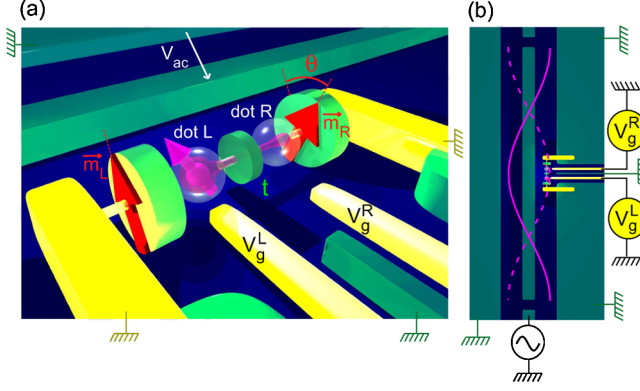assumptions, the simplified double dot Hamiltonian writes

FIG. 1 (color online). (a) The two quantum dots L and R (transparent spheres) are connected together through a tunnel junction with hoping constant t (small green disk). Each dot is connected to a grounded normal reservoir (yellow rectangle) through a ferromagnetic insulator (FI) (large green disks). The magnetizations $\vec{m}_L$ and $\vec{m}_R$ of the two FIs (red arrows) form an angle θ. The double dot circuit is placed between the center and ground conductors of a superconducting coplanar waveguide (green tapes), which conveys a voltage V_{ac}. The dot $L(R)$ is capacitively coupled to a gate with voltage $V_g^{L(R)}$. We tune V_g^L and V_g^R such that there is a single active electron on the double dot system, mainly localized on dot L (magenta cloud). (b) Top view of the same device on a wider scale. The double dot is placed at an antinode of the cavity voltage standing wave. For clarity we have not respected the relative scales.
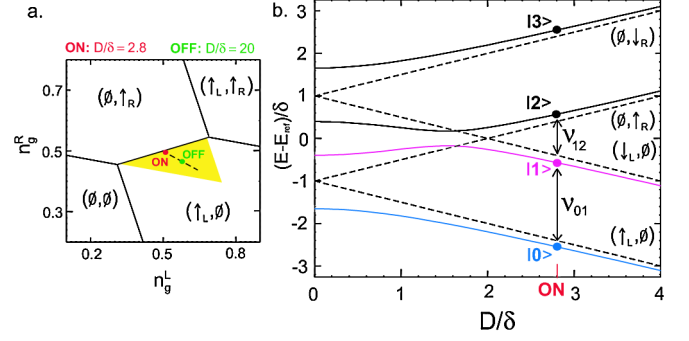

FIG. 2 (color online). (a) Stability diagram indicating the double dot most stable state for $t = 0$, versus the reduced gate voltages $n_g^{L(R)} = C_g^{L(R)} V_g^{L(R)}/e$. We have used the capacitance values indicated in the supplementary material [21], and $V_{ac} = 0$. The circuit can be operated along the dashed line $n_g^R = 0.5 + [(C_\Sigma^R + C_m)/(C_\Sigma^L + C_m)](0.5 - n_g^L)$ to maximize the energy separation between the singly occupied levels $|\varnothing, \uparrow_R\rangle, |\varnothing, \downarrow_R\rangle, |\uparrow_L, \varnothing\rangle$ and $|\downarrow_L, \varnothing\rangle$ and other energy levels corresponding to a different double dot occupation. This yields a detuning $D = e^2(2n_g^L - 1)/(C_\Sigma^L + C_m)$ between the states $|\uparrow_L, 0\rangle$ and $|0, \uparrow_R\rangle$. (b) Eigenenergies of the double dot versus D for $\delta = 16~\mu$eV, $\theta = \pi/6$, $t = 0$ (dashed lines), and $t = 2\delta/3$ (solid lines). When $t = 0$, the levels $|\downarrow_L, 0\rangle$ and $|0, \uparrow_R\rangle$ cross at $D = 2\delta$. This crossing is replaced by an anticrossing for $t \neq 0$ and $\theta \neq 0[2\pi]$. At $t = 2\delta/3$, $D = 2.8\delta$ and $\theta = \pi/6$ (on point), we obtain transition frequencies $\nu_{01} = 7.68$ GHz and $\nu_{12} = 4.41$ GHz.

$$\hat{H} = -\frac{D}{2}\hat{\tau}_3\hat{\sigma}_0 + t\hat{\tau}_1\hat{\sigma}_0 - \delta_L\hat{\sigma}_3\frac{\hat{\tau}_0 + \hat{\tau}_3}{2}$$
$$- \delta_R[\cos(\theta)\hat{\sigma}_3 + \sin(\theta)\hat{\sigma}_1]\frac{\hat{\tau}_0 - \hat{\tau}_3}{2}. \quad (1)$$

Here, $\hat{\tau}_i$ and $\hat{\sigma}_i$, with $i \in \{0, 1, 2, 3\}$, refer to the identity and Pauli matrices in the left or right orbital subspace and the ($\uparrow_L$, $\downarrow_L$) spin subspace, respectively. We note D the energy shift between the states $|\uparrow_L, \varnothing\rangle$ and $|\varnothing, \uparrow_R\rangle$ for $t = 0$. This quantity can be tuned with the dots' gate voltages [21]. For simplicity, we assume $\delta_L = \delta_R = \delta$. We define an "on" working point $D = D_{ON} = 2.8\delta$, with $\theta = \pi/6$, $t = 2\delta/3$ and $\delta = 16~\mu$eV $\simeq 3.9$ GHz. At the on point, we note $|\mathbf{j}\rangle$, with $\mathbf{j} \in \{1, 2, 3, 4\}$, the eigenstates of $\hat{H}$, with energies $E_{\mathbf{j}}$ growing with the index $\mathbf{j}$. The two lowest eigenstates $|0\rangle$ and $|1\rangle$ both have an overlap to the right dot of only $\sim 5\%$, and they correspond to $\uparrow_L$ and $\downarrow_L$ spin states to a good approximation since we obtain $|\langle\varnothing, \downarrow_L|0\rangle|^2 = 0.05\%$, $|\langle\downarrow_L, \varnothing|0\rangle|^2 = 0.005\%$, $|\langle\varnothing, \uparrow_L|1\rangle|^2 = 0.8\%$ and $|\langle\uparrow_L, \varnothing|1\rangle|^2 = 0.1\%$. We obtain a transition frequency $\nu_{01} = (E_1 - E_0)/h \simeq 1.98\delta = 7.68$ GHz accessible with current microwave technology. Importantly, the transition frequency $\nu_{12} = (E_2 - E_1)/h = 4.41$ GHz between the states $|1\rangle$ and $|2\rangle$ is significantly different from ν_{01}. The double dot circuit is thus sufficiently anharmonic to be operated as an effective two level system $\{|0\rangle, |1\rangle\}$, called "spin qubit" in the following. When D is changed to $D = D_{ON} + \delta D$ and $\theta \neq 0[\pi]$, one obtains a coupling element $\langle 0|\hat{H}|1\rangle = \mathcal{C}\delta D$ because the direction of the overall field felt by the electron

slightly changes. Importantly, when the capacitances connected to dots L and R are asymmetric, one has $\partial D/\partial V_{ac} \neq 0$ [21]. This property combined with $\mathcal{C} \neq 0$ allows a transverse coupling of the spin qubit to the electric field conveyed by the waveguide. In these conditions, Rabi oscillations between the states $|0\rangle$ and $|1\rangle$ can be obtained by applying an oscillating voltage with frequency ν_{01} to the waveguide center conductor. Using the rotating wave approximation and the quantization rule $V_{ac} = V_{rms}(a + a^\dagger)$ [22], with a, $a^\dagger$ the annihilation and creation operators for photons of the waveguide cavity, the set of the spin qubit and cavity can be described with a standard Jaynes-Cummings Hamiltonian $\hat{H}_{eff} = -h\nu_{01}\hat{S}_z/2 + \hbar\omega_r a^\dagger a + \hbar g(a^\dagger\hat{S}_- + a\hat{S}_+)$ with $\hbar g = \mathcal{C}V_{rms}\partial D/\partial V_{ac}$, $\hat{S}_\pm = (\hat{S}_x \pm i\hat{S}_y)/2$ and $\hat{S}_x$, $\hat{S}_y$, $\hat{S}_z$ the Pauli operators in the subspace $\{|0\rangle, |1\rangle\}$. Using realistic values for the circuit capacitances [21] and $V_{rms} = 2~\mu$V, we obtain a strong spin–electric-field coupling at the on point, i.e., $g/\pi = 5.6$ MHz in terms of vacuum Rabi frequency, a value comparable to that obtained in Ref. [5]. With such a coupling, the readout of the qubit state can be performed by measuring the dispersive shift of the cavity resonance frequency [22]. Besides, a distant coupling between two qubits can be realized by exchange of virtual cavity photons [23]. Importantly, our setup allows us to strongly decrease the spin-cavity coupling by increasing D. For instance, we obtain $g/\pi = 13$ kHz at the off point $D = D_{OFF} = 20\delta$ where $\nu_{01} \simeq 2\delta = 7.76$ GHz. Outside the qubit manipulation stage, the qubit can be placed at the off point to minimize

decoherence due to the coupling to the cavity [24]. This also allows us to switch off very efficiently the coupling between two qubits via virtual cavity photons, with almost no change of the qubit transition frequency. Then, the qubit has to be placed at the on point for the manipulation of its quantum state. This can be performed by using appropriate gate voltage pulses. Note that g also depends on the angle θ as shown in Fig. 3(a). However, using a constant θ imposed, e.g., by the shape of the FI layers should be sufficient in practice.

Reaching the strong coupling regime requires that the coherence times of the spin and the cavity photons are longer than $1/g$. Since our setup does not use any external magnetic field, it is compatible with using a superconducting cavity with a good quality factor. Nevertheless, the coherence time of the spin qubit can be limited by various mechanisms causing dephasing and relaxation. These mechanisms depend on the structural properties of the nanoconductors used. In principle, our scheme can be implemented with various types of nanoconductors, such as, e.g., silicon nanowires [25,26] or single wall carbon nanotubes (SWNTs). So far, the latter are the most advanced nanoconductors for realizing our setup. Semiconducting SWNTs are particularly suitable for defining double quantum dots, using top gates which allow one to tune the interdot coupling t [27]. Contact-induced Zeeman effective fields have already been observed in SWNTs [16,17]. Besides, multidot systems with ferromagnetic leads and a local gate control have already been realized in the open regime [28]. We consider a SWNT above which several gates and contacts are evaporated (inset of Fig. 4). The central electrostatic gate enclosing an insulating layer Is is used to define t. The two dots are delimited by Is and two other gates which enclose ferromagnetic insulating layers FI1 and FI2. Here, the role of the FI layers of our generic setup is played by the SWNT sections below FI1 and FI2. Following the approach of Ref. [29], these SWNT sections are subject to an effective
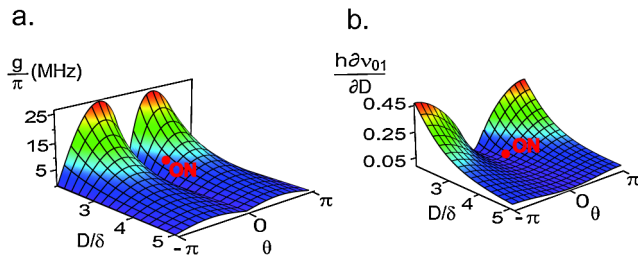
Zeeman field E_{ex}. The electron confined in dot $L(R)$ feels E_{ex} through its evanescent tail, which leads to $\delta_{L(R)} \neq 0$. We describe the electronic bands of the SWNT with the Dirac-like Hamiltonian

$$H_W = -i\hbar v_F \left(\frac{\hat{s}_1 \hat{\gamma}_3}{R} \frac{\partial}{\partial \varphi} + \hat{s}_2 \frac{\partial}{\partial \xi} \right) + \Delta_{K-K'} \hat{\gamma}_1 - E_{pot}(\xi). \quad (2)$$

Here, $\hat{s}_i$ and $\hat{\gamma}_i$ with $i \in \{1, 2, 3\}$ are the Pauli matrices on the A/B atoms and K/K' valley subspaces, R is the radius of the SWNT and $v_F = 810^5 \text{ m} \cdot \text{s}^{-1}$ is the SWNT Fermi velocity. The term $\Delta_{K-K'} \sim 3$ meV describes a coupling between the K and K' bands, responsible for an orbital level splitting currently observed in experiments [30,31]. We note ξ and φ the longitudinal and azimuthal SWNT coordinates. To obtain the spectral properties of dots L and R separately ($t = 0$), we use $E_{pot}(\xi < 0) = \sigma E_{ex}/2 + E_b$, $E_{pot}(0 < \xi < \lambda) = E_g^L$ and $E_{pot}(\xi > \lambda) = E_{Is}$ for dot L, and $E_{pot}(\xi < a + \lambda) = E_{Is}$, $E_{pot}(a + \lambda < \xi < a + 2\lambda) = E_g^R$, and $E_{pot}(\xi > a + 2\lambda) = \sigma E_{ex}/2 + E_b$ for dot R. These potential profiles can be adjusted with the various electrostatic gates shown in Fig. 4. Remarkably, we find that $\delta^{L(R)}$ depends on E_{ex}, but also on the size and the active orbitals of dots $L(R)$. Therefore, our scheme can work for a wide range of E_{ex} because $\delta^{L(R)}$ can be easily adjusted to the value $\sim 16 \mu$eV required in the generic model. Here, we use $E_{ex} = 3.7$ meV, consistently with Ref. [29], $R = 1$ nm and $\lambda = 100$ nm. We define the states $|\uparrow_L, \varnothing\rangle$ and $|\downarrow_L, \varnothing\rangle$ [$|\varnothing, \uparrow_R\rangle$ and $|\varnothing, \downarrow_R\rangle$] as the 29th lowest pair of spin-dependent levels in the conduction band of dot $L[R]$. Remarkably, for $E_b - E_g^L \sim 1.05\Delta_{SWNT}$, with
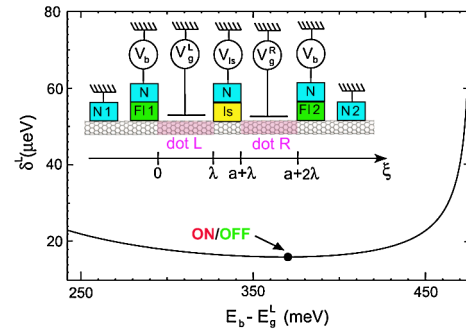
FIG. 4 (color online). Inset: Implementation of our setup with a SWNT. The dots L and R are delimited by the gates enclosing the insulating layer Is and the ferromagnetic insulators FI1 and FI2. The outer normal metal contacts $N1$ and $N2$ are used to control the dots' occupation numbers. Main frame: Half-effective Zeeman splitting δ^L calculated for dot L in the framework of Eq. (2), with $|\uparrow_L, \varnothing\rangle$ and $|\downarrow_L, \varnothing\rangle$ corresponding to the 29th lowest pair of spin-dependent levels in the dot conduction band. This quantity depends on the chemical potential shift $E_b - E_g^L$ between dot L and the neighboring SWNT sections. We obtain a sweet spot $\partial \delta^L / \partial E_g^L = 0$ (black point) which can be used to reduce charge noise-induced dephasing mediated by fluctuations of δ^L. In this Figure, we use $E_b = E_{Is}$, $R = 1$ nm, $\lambda = 100$ nm, and $E_{ex} = 3.7$ meV.

FIG. 3 (color online). (a) Spin–electric-field coupling g of the spin qubit, in terms of vacuum Rabi frequency g/π. This quantity decreases with D, vanishes for $\theta = 0[\pi]$, and reaches a maximum for values $\theta = \pm \theta_{max}(D)$ close to $\pm \pi/2$. At the on point ($D = 2.8\delta$, $\theta = \pi/6$), we obtain $g/\pi = 5.6$ MHz. At the off point ($D = 20\delta$, $\theta = \pi/6$), which is indicated in Fig. 2(a), we obtain $g = 13$ kHz. (b) Derivative of the transition frequency ν_{01} with respect to D. This quantity mainly determines the sensitivity of the qubit to charge noise mediated by fluctuations of D.

$\Delta_{\text{SWNT}} = 350$ meV the SWNT band gap, we obtain a sweet spot $\partial \delta^L / \partial E_g^L = 0$, with $\delta^L = 16$ μeV. One has $E_g^R - E_g^L \ll E_b - E_g^{R(L)}$ at the on and off points, thus $\delta^R \sim \delta^L$. Finally, the interdot coupling t can be calculated from the overlap between the dots' orbitals. The value $t = 2\delta/3$ can be obtained by varying a and E_{Is}, without affecting significantly the sweet spot (not shown).

The spin coherence time is expected to be comparably long in SWNTS. Current estimates based on the spin-orbit interaction in ^{13}C-free SWNTs lead to milliseconds [32]. Since our setup provides a new way to control the spin degree of freedom, it is *a priori* subject to specific decoherence mechanisms which we evaluate below. First, low frequency charge noise picked up by the dot gates risks to induce fluctuations of D and thus ν_{01}, which will limit the spin dephasing time T_φ^D. Since $\partial \nu_{01}/\partial D$ decreases with D, the choice of D_{ON} results from a compromise between having a low T_φ^D and a large g. This compromise also requires us to use a relatively small value for θ, although g is maximal for values of θ close to $\pm \pi/2$ [see Fig. 3(b)]. Using a semiclassical approach, we estimate $T_\varphi^D \sim 2.9$ μs and $T_\varphi^D \simeq 2$ ms at the on and off points, using the charge noise amplitude measured in nonsuspended SWNTs [33]. Second, from Eq. (1), ν_{01} corresponds to $\sim 2\delta^L$. Hence, charge noise can also dephase the qubit through fluctuations of δ_L. However, it is possible to minimize this effect by working at the sweet spot $\partial \delta_L / \partial E_g^L = 0$ in both the on and off states (see Fig. 4). This gives a dephasing time $T_\varphi^{\delta_L} = 15$ ms $\gg T_\varphi^D$. Third, the electron-phonon interaction conserves spin. However, since the states $|0\rangle$ and $|1\rangle$ have slight components in $\downarrow_L$ and $\uparrow_L$ respectively, they can relax due to electron-phonon interaction. To evaluate this effect, we take into account the acoustic mode most strongly coupled to electrons, i.e., the stretching mode [34]. We assume that the phonons in dots L and R are confined and decoupled due to the massive top gates. We obtain $T_1^{\text{ON}} = 1.0$ μs and $T_1^{\text{OFF}} = 0.21$ s at the on and off point respectively [21]. Quite generally, using suspended nanoconductors could reduce further decoherence, by decreasing the charge noise picked up by the device, and also by reducing the phonon-induced T_1 thanks to a phononic Purcell-like effect. For instance, we estimate $T_1^{\text{ON}} \simeq 14$ μs and $T_1^{\text{OFF}} \simeq 2.8$ s in the SWNT setup, for phonons confined inside dots L and R with a quality factor $Q_{\text{ph}} = 20$. In principle, one can also expect relaxation due to the coupling to the cavity, similar to what is observed with superconducting qubits [24]. However, at the off point, we expect the cavity to be a marginal source of decoherence since g is almost switched off. At the on point, it is in principle possible to reduce the cavity-induced relaxation by improving the cavity design [35]. Hence, we have focused on decoherence sources more specific to our qubit design. In summary, for a nonsuspended SWNT setup, we finally obtain a promising total decoherence time

$T_2^{\text{ON}} = 1.2$ μs $\gg 1/g = 177$ ns   at   the   on   point. Remarkably, at the off point, we obtain $T_2^{\text{OFF}} \simeq 2$ ms while g is reduced by a factor of 450 compared to the on point. This suggests that our spin qubit could also be used as a quantum register.

[1] H. Mabuchi and A. Doherty, Science **298**, 1372 (2002).
[2] J. M. Raimond, M. Brune, and S. Haroche, Rev. Mod. Phys. **73**, 565 (2001).
[3] T. Yoshie *et al.*, Nature (London) **432**, 200 (2004).
[4] J. P. Reithmaier *et al.*, Nature (London) **432**, 197 (2004).
[5] A. Wallraff *et al.*, Nature (London) **431**, 162 (2004).
[6] R. Hanson *et al.*, Rev. Mod. Phys. **79**, 1217 (2007).
[7] L. Childress, A. S. Sørensen, and M. D. Lukin, Phys. Rev. A **69**, 042302 (2004).
[8] Y. Tokura *et al.*, Phys. Rev. Lett. **96**, 047202 (2006).
[9] K. C. Nowack *et al.*, Science **318**, 1430 (2007).
[10] M. Trif *et al.*, Phys. Rev. Lett. **101**, 217201 (2008).
[11] M. Trif, V. N. Golovach, and D. Loss, Phys. Rev. B **77**, 045434 (2008).
[12] G. Burkard and A. Imamoglu, Phys. Rev. B **74**, 041307(R) (2006).
[13] L. Frunzio *et al.*, IEEE Trans. Appl. Supercond. **15**, 860 (2005).
[14] S. M. Girvin, M. H. Devoret, R. J. Schoelkopf, Phys. Scr. **T137**, 014012 (2009).
[15] A. Cottet and M.-S. Choi, Phys. Rev. B **74**, 235316 (2006).
[16] S. Sahoo *et al.*, Nature Phys. **1**, 99 (2005).
[17] J. R. Hauptmann, J. Paaske, and P. E. Lindelof, Nature Phys. **4**, 373 (2008).
[18] K. Hamaya *et al.*, Appl. Phys. Lett. **91**, 022107 (2007).
[19] P. M. Tedrow, J. E. Tkaczyk, and A. Kumar, Phys. Rev. Lett. **56**, 1746 (1986).
[20] A. Cottet *et al.*, Phys. Rev. B **80**, 184511 (2009).
[21] See supplementary material at http://link.aps.org/supplemental/10.1103/PhysRevLett.105.160502.
[22] A. Blais *et al.*, Phys. Rev. A **69**, 062320 (2004).
[23] J. Majer *et al.*, Nature (London) **449**, 443 (2007).
[24] A. A. Houck *et al.*, Phys. Rev. Lett. **101**, 080502 (2008).
[25] N. Shaji *et al.*, Nature Phys. **4**, 540 (2008).
[26] B. T. Jonker *et al.*, Nature Phys. **3**, 542 (2007).
[27] N. Mason, M. J. Biercuk, and C. M. Marcus, Science **303**, 655 (2004).
[28] C. Feuillet-Palma *et al.*, Phys. Rev. B **81**, 115414 (2010).
[29] H. Haugen, D. Huertas-Hernando, and A. Brataas, Phys. Rev. B **77**, 115406 (2008).
[30] W. Liang, M. Bockrath, and H. Park, Phys. Rev. Lett. **88**, 126801 (2002).
[31] S. Sapmaz *et al.*, Phys. Rev. B **71**, 153402 (2005).
[32] D. V. Bulaev, B. Trauzettel, and D. Loss, Phys. Rev. B **77**, 235301 (2008).
[33] L. G. Herrmann *et al.*, Phys. Rev. Lett. **99**, 156804 (2007).
[34] H. Suzuura and T. Ando, Phys. Rev. B **65**, 235412 (2002).
[35] H. Wang *et al.*, arXiv:0909.0547.